Fluid Phase Equilibria 596 (2025) 114429

Contents lists available at ScienceDirect

Fluid Phase Equilibria

journal homepage: www.journals.elsevier.com/fluid-phase-equilibria

Thermal and mutual diffusivities in binary mixtures of alkanes with dissolved gases by dynamic light scattering (DLS)

Chathura J. Kankanamge [a], Paul Damp [a], Thomas M. Koller [a], Michael H. Rausch [a], Dominik Krug [b], Wolfgang Schröder [b,c], Tobias Klein [a], Andreas P. Fröba [a,*]

[a] Institute of Advanced Optical Technologies – Thermophysical Properties (AOT-TP), Department of Chemical and Biological Engineering (CBI) and Erlangen Graduate School in Advanced Optical Technologies (SAOT), Friedrich-Alexander-Universität Erlangen-Nürnberg (FAU), Paul-Gordan-Straße 8, 91052 Erlangen, Germany
[b] Chair of Fluid Mechanics and Institute of Aerodynamics (AIA), Faculty of Mechanical Engineering, RWTH Aachen University, Wüllnerstraße 5a, 52062 Aachen, Germany
[c] JARA Center for Simulation and Data Science, RWTH Aachen University, Seffenter Weg 23, 52074 Aachen, Germany

ARTICLE INFO

Keywords:
Fick diffusion coefficient
Thermal diffusivity
Binary mixtures
Alkanes
Carbon dioxide
Propane
Dynamic light scattering (DLS)

ABSTRACT

This work presents thermal diffusivities a and Fick diffusion coefficients D_{11} of binary mixtures of the alkanes *n*-pentane, *n*-decane, *n*-hexadecane, or squalane (2,6,10,15,19,23-hexamethyltetracosane) with dissolved carbon dioxide (CO_2) or propane by dynamic light scattering (DLS). The investigations are performed over a temperature range from (293 to 393) K and cover a wide composition range from infinite dilution of the dissolved gas up to an amount fraction of the gas of 0.69. Using DLS, D_{11} and a are accessed with average expanded experimental uncertainties (coverage factor $k = 2$) of (6.6 and 7.6)%. The results from this work are compared to the few experimental data available in the literature and are used to investigate the influences of the thermodynamic state and of the characteristics of the solvent and solute molecules on both transport properties. For all investigated binary mixtures, the influence of the dissolved gas on a is found to be small since most data agree with a of the pure solvent within combined uncertainties. The composition-dependent trend for D_{11} varies strongly for the different binary mixtures, where both an increase or decrease with increasing amount fraction of the dissolved gas can be observed. For D_{11} at infinite dilution, two prediction models from the literature are tested. While both models are able to qualitatively predict the temperature-dependent trend of D_{11}, the relative deviation of the predicted D_{11} from the present experimental results varies strongly for the different mixtures between (9 and 95)%.

1. Introduction

Compressors in the form of rotary positive displacement machines are part of many cycles, such as heat pump and refrigeration cycles. Since the power requirement of compressors enters directly into the calculation of the efficiency of the corresponding cycles, the reliable design of compressors is indispensable for the optimization of complete cycles. This requires a fundamental understanding of the surge and gap flow between the moving rotator and the static housing in rotary positive displacement machines. Therefore, it is the overarching aim of the Research Unit "FOR 5595: Oil-refrigerant multiphase flows in gaps with moving boundaries – Novel microscopic and macroscopic approaches for experiment, modeling, and simulation (ARCHIMEDES)", which is funded by the German Research Foundation (Deutsche Forschungsgemeinschaft, DFG), to contribute to a better understanding of how the surge and gap flow can be characterized. Assessing this flow field experimentally is highly challenging, which makes it necessary to use direct numerical simulations to aid in unraveling the complexity of the flow. The gas mass flow through the sealing gaps as well as momentum losses due to friction are of particular interest. One key aspect of the sealing gap flow is the evolution of entrapped and transported gas bubbles. Over the length of the sealing gap, the bubbles experience a pressure gradient due to adjacent high- and low-pressure regions, which leads to expansion of these bubbles. Additionally, dissolved gas from the liquid phase is transferred to the gas phase by diffusion, which further enhances the bubble growth. The temperature distribution within the gap affects properties such as the fluid's dynamic viscosity and the gas density, making the conduction of heat an important aspect of the

* Corresponding author.
E-mail address: andreas.p.froeba@fau.de (A.P. Fröba).

https://doi.org/10.1016/j.fluid.2025.114429
Received 3 February 2025; Received in revised form 13 March 2025; Accepted 17 March 2025
Available online 18 March 2025
0378-3812/© 2025 The Author(s). Published by Elsevier B.V. This is an open access article under the CC BY license (http://creativecommons.org/licenses/by/4.0/).

problem. To be able to represent these processes accurately in direct numerical simulations, the accurate knowledge of thermophysical properties and, especially, the transport properties of the fluid present in the gap are to be considered. In refrigeration cycles, the fluid in the gap is a mixture consisting of the lubrication or refrigeration oil with dissolved working fluid of the cycle, i.e. the refrigerant. This means that for performing direct numerical simulations, the thermophysical properties of the refrigeration oil–refrigerant mixture are required, but are often not available in the literature, in particular for the model systems investigated in the present study.

In this work, experimental data for the transport properties thermal diffusivity a and Fick diffusion coefficient D_{11} are presented for surrogate refrigeration oil–refrigerant mixtures over wide ranges of temperature and composition. These mixtures consist of the alkanes *n*-pentane, *n*-decane, *n*-hexadecane, or squalane as surrogates for the refrigeration oil and carbon dioxide (CO_2) or propane as representatives for the refrigerants. By this, pairs of varying asymmetry between the molecular sizes of the refrigeration oil and the refrigerant can be mapped. Experimental results for a and D_{11} in the liquid phase are obtained at vapor-liquid equilibrium by DLS experiments, which allows their reliable determination in macroscopic thermodynamic equilibrium without the need of calibration by studying statistical fluctuations in temperature or entropy and composition. The results from this work are compared to the very limited amount of experimental data available in the literature and are discussed with respect to the influences of the thermodynamic state and characteristics of the refrigeration oil and refrigerant as solvent and solute.

2. Methods

2.1. Materials and sample preparation

This study investigates binary mixtures consisting of the solvents *n*-pentane, *n*-decane, *n*-hexadecane, or squalane with the dissolved gases carbon dioxide (CO_2) or propane. The investigations include concentrations ranging from the infinite dilution of the dissolved gas up to an amount fraction of the gas $x_{gas} = 0.69$ within the temperature range $T =$ (293.15 to 393.15) K. The purity of the substances studied as well as their suppliers are given in Table 1.

In the following, the sample preparation is shortly described. To remove particle-like impurities that may be present in the pure solvents and could interfere with the reliable determination of the properties of interest, the solvents *n*-decane, *n*-hexadecane, and squalane were filtered using a stack of two poly(tetrafluoroethylene) (PTFE) syringe filters with pore sizes of 200 nm and 450 nm at ambient conditions, i.e. at a pressure p of 0.1 MPa and a temperature T of 293 K. Since preliminary investigations within a cuvette had shown no particle-like impurities present in *n*-pentane, it was used without filtration. Afterwards, about 20 mL of the solvent was filled into a stainless-steel sample cell with a total inner volume of about 32 mL and four optical accesses. To remove highly volatile components such as air, the solvent in the sample cell was degassed by reducing p inside the cell using an oil-sealed vacuum pump. For *n*-pentane, which has a relatively high vapor pressure, vacuum was applied only shortly to purge the vapor phase. To obtained the desired saturation pressure p_{sat}, corresponding to a desired amount fraction of the gas dissolved in the liquid phase, x_{gas}, CO_2 or propane was then injected into the sample cell. Here, x_{gas} is estimated based on the solubility data available in the literature according to the procedure described in Section 3.3.

2.2. Dynamic light scattering

Dynamic light scattering (DLS) analyses the dynamics of the scattered light intensity originating from a fluid irradiated with coherent laser light at macroscopic thermodynamic equilibrium. The dynamics of the scattered light intensity reflect those of microscopic fluctuations in T or entropy, p, and, in the case of mixtures, concentration c [1]. Through the computation of the normalized second-order correlation function (CF), $g^{(2)}(\tau)$, as a function of the correlation time τ, DLS provides access to the mean lifetime of these fluctuations and, thus, to the associated transport properties in an absolute manner without the need for calibration. Neglecting fluctuations in p and ensuring a heterodyne detection scheme, where the scattered light is superimposed by a local oscillator field of much stronger intensity, the CF related to a binary mixture is given by

$$g^{(2)}(\tau) = b_0 + b_t \exp\left(-|\tau|/\tau_{C,t}\right) + b_c \exp\left(-|\tau|/\tau_{C,c}\right). \quad (1)$$

In Eq. (1), b_0, b_t, and b_c are constants and depend on the experimental boundary conditions, for instance, the experimental setup, the thermodynamic state, and the local oscillator field. The mean lifetimes of fluctuations in T and c are represented by $\tau_{C,t}$ and $\tau_{C,c}$, which can be related to the thermal diffusivity a and the Fick diffusion coefficient D_{11} via $a = 1/(\tau_{C,t} \cdot q^2)$ and $D_{11} = 1/(\tau_{C,c} \cdot q^2)$. Here, coupling effects of the hydrodynamic modes related to T and c fluctuations are neglected, which is safely valid for the present study [2]. q denotes the modulus of scattering vector according to $q = (4\pi \cdot n_{fluid}/\lambda_0) \cdot \sin(\Theta_S/2)$. With the help of the Snell's refraction law, the scattering angle Θ_S can be expressed by the incident angle Θ_i, which is defined by the direction of the incident light and that of the detected scattered light. n_{fluid} is the refractive index of the fluid at the wavelength of the laser in vacuo λ_0. Within this study, Θ_i was varied between (3 and 9)°. For such small Θ_i, a change of n_{fluid} even by 300% would only change the corresponding diffusivities by approximately 0.8% [3], which is clearly within their experimental uncertainties. Therefore, n_{fluid} of the pure solvents [4–6] were used for the evaluation of D_{11} and a in the binary mixtures. For a more detailed description and the theoretical basis of DLS, the reader is referred to the literature [1,7–9].

The experimental and electronic setup as well as the T and p sensors used are identical to those described in previous publications, e.g., in Ref. [10]. During DLS experiments, T and p were measured continuously with absolute uncertainties ($k = 2$) of 20 mK and 0.008 kPa. The scattered light was collected under a heterodyne detection scheme by two photo multiplier tubes (PMTs). To limit artefacts like deadtime and after-pulsing effects, the two PMTs are operated in a pseudo cross-correlation scheme. The CFs are then computed by two correlators, which are a linear-tau correlator with 2047 equally spaced channels and

Table 1
Specification of the chemical supplier, molar mass M, and mass fraction w_i or volume fraction ϕ_i purities of the solvents and solutes.[a]

component	CAS reg. no.	source	M / (g·mol^{-1})	purity in w or ϕ
n-pentane (*n*-C_5H_{12})	109–66–0	Thermo Fisher Scientific	72.15	$w \geq 0.99$
n-decane (*n*-$C_{10}H_{22}$)	124–18–5	Thermo Fisher Scientific	142.28	$w \geq 0.992$
n-hexadecane (*n*-$C_{16}H_{34}$)	544–76–3	Thermo Fisher Scientific	226.44	$w \geq 0.985$
squalane ($C_{30}H_{62}$)	111–01–3	Thermo Fisher Scientific	422.81	$w \geq 0.985$
carbon dioxide (CO_2)	124–38–9	AIR LIQUIDE	44.01	$\phi \geq 0.99995$
propane (C_3H_8)	74–98–6	TEGA - Technische Gase und Gasetechnik GmbH	44.10	$w \geq 0.995$

[a] Sample purities in form of w_i or ϕ_i are given as specified in the certificates of analysis by the manufacturers.

a multi-tau correlator with a logarithmic time structure featuring 263 channels. The mean lifetimes of the fluctuations, $\tau_{C,t}$ and $\tau_{C,c}$, and the experimental constants are determined through least-squares fitting of the recorded CFs to Eq. (1). In addition to the experimental signals associated with fluctuations in T and c, the recorded CFs may contain other disturbing or long-term signals. These can arise from external stray light in the laboratory, particle-like impurities in the samples, and/or dust on the mirrors. Consequently, additional first-order or second-order polynomial functions as function of τ are included in Eq. (1) to account for these long-term signals in the CFs if necessary. An example for an experimental CF recorded for a binary mixture of *n*-pentane with CO_2 at $T = 293.08$ K, $p_{sat} = 0.973$ MPa, and $\Theta_i = 4.469°$ is shown in Fig. 1. The measured signal can only be described by a sum of two exponentials according to Eq. 1, which reflect the faster signal related to a (green dashed line) and the slower signal related to D_{11} (blue dotted line). The residual plot in the bottom part of Fig. 1 indicates that the theoretical working equation, Eq. (1), represents the measurement signal accurately.

To ensure that the obtained τ_C data relate to the transport properties a and D_{11}, it must be verified that the resolved fluctuations originate from hydrodynamic fluctuations. According to the theory of hydrodynamic fluctuations, this is possible through checking the relationship between the inverse of the mean lifetime of fluctuations and the squared modulus of the scattering vector, q^2 [11]. For hydrodynamic fluctuations, this relationship is linear and crosses the origin of a corresponding diagram, where the slope determines the magnitude of the associated transport property. Such a representation is exemplarily shown in Fig. 2 for the mixture consisting of *n*-decane and CO_2 at $T = 292.96$ K and $p_{sat} = 2.97$ MPa. Here, a green solid and a blue dotted line represent the linear fits of $\tau_{C,t}^{-1}$ and $\tau_{C,c}^{-1}$ with respect to q^2. During the fitting procedure, the individual datapoints were weighted by the inverse of their uncertainties and the fits were not forced to intersect with the origin. Considering the experimental uncertainties, both linear fits pass through the origin, confirming that the resolved signals are associated with hydrodynamic fluctuations. The values for a and D_{11} calculated from the slopes of the two fits are shown in Fig. 2 and deviate by (0.2 and 0.7)% from the average values of the five individual measurements.

2.3. Mixture composition

Although it is not necessary to know the liquid-phase composition of a mixture for the measurement of a and D_{11} by DLS, it must be known to identify any relations between composition and the transport properties. Therefore, the estimation of the liquid mixture compositions studied by DLS based on corresponding solubility data performed within this work is explained in the following. Since the amount of appropriate solubility data in the literature is limited for the present systems, the estimated compositions are subjected to rather large uncertainties. For all results from this work, T and p are given aside from the estimated compositions. This will allow to determine more accurate amount fractions of the components in the future when further solubility data or equations of state become available.

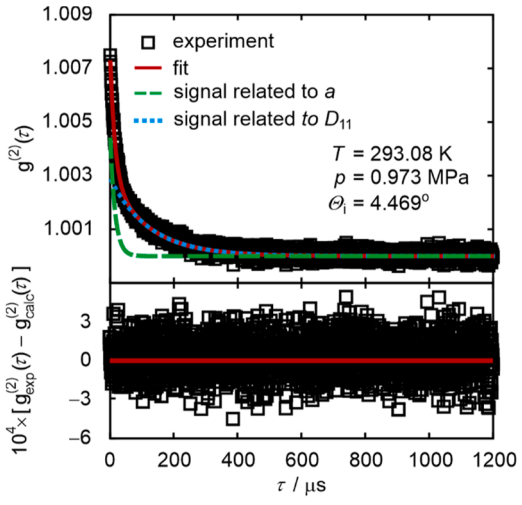

Fig. 1. CF recorded for a mixture consisting of *n*-pentane and dissolved CO_2 at $T = 293.08$ K, $p_{sat} = 0.973$ MPa, and $\Theta_i = 4.469°$ (top) and the residuals from the fit (bottom). The red solid line represents the global fit according to Eq. (1). The signals related to a and D_{11} are shown by a green dashed and a blue dotted line.

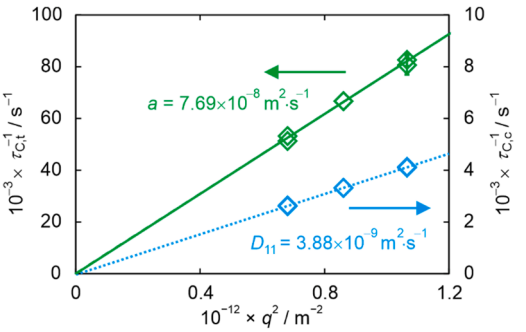

Fig. 2. Inverse of the mean lifetime of fluctuations in temperature, $\tau_{C,t}^{-1}$, or concentration, $\tau_{C,c}^{-1}$, as a function of the squared modulus of the scattering vector, q^2, for the mixture consisting of *n*-decane and dissolved CO_2 at $T = 292.96$ K and $p_{sat} = 2.97$ MPa. Symbols represent the experimentally determined values and error bars indicate their expanded experimental uncertainties ($k = 2$), which are shown only if they are larger than the symbols. The green solid and the blue dotted line represent the linear fits of $\tau_{C,t}^{-1}$ or $\tau_{C,c}^{-1}$.

For calculating the composition during the DLS experiments, the relationship between the partial pressure of the dissolved gas, i.e. the solute, and its amount fraction in the liquid phase according to the literature data was described at a given T according to

$$x_{gas} = H_{12}(p - p_{solvent}). \tag{2}$$

Here, H_{12} is the proportionality constant at a given T, similar to Henry's law constant. The partial pressure of the solute in the gas phase is assumed to be $p_{gas} = p - p_{solvent}$, where $p_{solvent}$ is assumed to be the vapor pressure of the pure solvent at T. The data for $p_{solvent}$ were taken from equations of state implemented in the REFPROP database [12] in the cases of *n*-pentane [13], *n*-decane [14], and *n*-hexadecane [15], or from the literature in the case of squalane [16]. The determined values for H_{12} were fitted as a function of T for a given mixture according to [7,17]

$$H_{12} = A + \frac{B}{T} + C \cdot \ln(T). \tag{3}$$

Here, the obtained parameters A, B, and C are mixture-specific.

Table 2 summarizes the solubility data from the literature in terms of the amount fraction of the dissolved gas in the liquid phase that were considered for the determination of H_{12}. The table also shows the corresponding ranges in T, p, and composition, number of data points, and a statistical comparison between the experimental data and the correlation according to Eqs. (2) and (3). This comparison includes the average absolute deviation (AAD) and the maximum deviation (Δ_{max}) of the literature data from the correlation.

For the binary mixtures *n*-decane/propane, *n*-decane/CO_2, and *n*-pentane/CO_2, the available solubility data cover the T and p ranges that were investigated in this work and no extrapolation was necessary. In the case of *n*-hexadecane/propane, H_{12} data were directly provided by the literature. These values were used within the specified T range and extrapolated from (302 to 293) K. In the case of *n*-pentane/propane, H_{12}

Table 2
Summary of the experimental data considered for the correlation of the solubilities according to Eqs. (2) and (3). The AAD and Δ_{max} represent absolute deviations of x_{gas} of the literature data from the correlation.

solvent	T / K	p / MPa	x_{gas}	number of data points	AAD	Δ_{max}	Refs.
CO_2-based mixtures							
n-pentane	252.7–394.3	0.159–5.96	0.006–0.321	65	0.0035	0.0069	[18]
n-decane	266.5–410.9	0.00003–5.52	0–0.422	25	0.0034	0.0157	[19]
squalane	298.6–330.2	0.1	-	11	0.0048	0.0098	[20]
propane-based mixtures							
n-pentane	336.6–373.2	0.334–0.59	0.047–0.54	33	0.0052	0.0090	[21]
n-decane	227.6–410.9	0.00003–1.38	0–0.946	18	0.0099	0.0157	[22]
n-hexadecane	302.0–391.6	0.205–0.649	0.149–0.172	19	0.0087	0.0158	[23]
squalane	325.0–400.1	0.039–0.307	0.037–0.135	16	0.0008	0.0010	[24]

was extrapolated from (383 to 393) K. For squalane/propane, the two lowest investigated T and, in part, p ranges required extrapolation, as these fall outside the ranges of the available literature data. For squalane/CO_2, H_{12} was directly provided by the literature but required extrapolation to higher T and the lowest T over a wide p range. Therefore, caution is advised for the interpretation of the results for this system in these extrapolated ranges.

3. Results and discussion

3.1. Summary of the diffusivities measured by DLS

In this work, a and D_{11} of binary liquid mixtures consisting of the solvents *n*-pentane, *n*-decane, *n*-hexadecane, or squalane and the solutes CO_2 or propane are investigated by DLS experiments at T between (293.15 and 393.15) K over a wide composition range. The amount fraction of the solute gas in the liquid phase x_{gas} is varied by adjusting the saturation pressure p_{sat} between (0.1 and 5) MPa. The determined a and D_{11} for all investigated mixtures together with their expanded relative experimental uncertainties ($k = 2$) at each state point are summarized in Table 3. The uncertainties for a, $U_r(a)$, vary between (1.6 and 26)% and are about 7.6% on average. For D_{11}, the uncertainties $U_r(D_{11})$ range between (1.1 and 16)% with an average value of 6.6%. Additionally, the results for a and D_{11} for the binary mixture consisting of CO_2 and *n*-hexadecane measured by Piszko et al. [25] using DLS are used for the discussion.

For the mixtures based on *n*-pentane near infinite dilution of the dissolved gas, only the hydrodynamic mode related to a could be resolved at the highest investigated T. This limitation arises from the interplay between the Lewis number Le and the Rayleigh ratio $\mathcal{R}$. Le describes the ratio of a to D_{11}, while $\mathcal{R}$ represents the ratio of signal amplitudes related to fluctuations in c and T, i.e. $b_c \cdot b_t^{-1}$. In Fig. 3, Le is presented as a function of T for the mixture *n*-pentane/propane close to infinite dilution of the dissolved propane. It can be observed that Le decreases with increasing T. Extrapolating these values would yield Le values of (3.4 and 2.6) at $T = (373$ and $393)$ K, which should in principle make it possible to resolve both modes [26]. However, the average value for $\mathcal{R}$ for this system is found to be approximately 0.06 across the investigated T range, indicating that signal contributions related to c fluctuations are very weak compared to those associated with T fluctuations. As the mean lifetimes of the two modes approach each other in the CFs at higher T, the much stronger amplitude of the T mode complicates the reliable evaluation of the c mode with much weaker amplitude. Therefore, only one mode could be resolved at higher T for the *n*-pentane/propane mixtures. The justification that this resolved mode is indeed related to a and not to an effective diffusivity is further verified by comparing the determined a values with corresponding data obtained from the REFPROP database [12], where details are given in Section 3.2.

3.2. Thermal diffusivity

3.2.1. Influence of temperature at infinite dilution of the dissolved gas

Thermal diffusivities a for the seven studied mixtures close to infinite dilution of the solutes CO_2 or propane with $x_{gas} \approx 0.05$ are shown in Fig. 4 as a function of T. For clarity, error bars, representing the experimental uncertainties, that are smaller than the size of the symbols are not displayed. Different symbol types and colors indicate mixtures with different solvents, while open or filled symbols differentiate between mixtures containing propane or CO_2. The comparably larger error bars for a in mixtures with *n*-hexadecane or squalane are attributed to adjustments made to the spatial resolution in the CFs, which, in line with the objective of this study, maximizes the relevant information needed to access D_{11}.

Consistent with previous studies [32–34], a for all systems tends to decrease with increasing T. The lowest a at a given T can be observed in mixtures containing *n*-pentane, while the data for the mixtures with *n*-decane are significantly larger. However, clear statements regarding a for the mixtures based on *n*-hexadecane and squalane cannot be given due to their rather larger experimental uncertainties. At any given T, there is also no discernible difference in a of mixtures of a given solvent containing CO_2 or propane. Owing to the lack of experimental data in the literature for corresponding mixtures, a for the mixtures near infinite dilution are compared to a of the pure solvents as shown in Fig. 4. Respective values for the solvents *n*-pentane, *n*-decane, and *n*-hexadecane are obtained with data from the REFPROP database [12] according to $a = \lambda/(\rho \cdot c_p)$, calculated on the basis of density ρ and heat capacity c_p data from equations of state and of thermal conductivities λ [13–15,27–29]. a for the mixture deviates from these pure-solvent data with an average absolute relative deviation (AARD) of 2.6%, which clearly falls within the experimental uncertainties. Since no literature data for a of pure squalane could be found, a data for this solvent at $p = 0.1$ MPa are also calculated with the help of λ [30], ρ [31], and c_p [31] data. The calculated a data of squalane are depicted as a dashed line in Fig. 4. For squalane, a of the mixture measured by DLS deviates from the calculated values of the pure solvent with an AARD of 8.1%. Considering the experimental uncertainties for the mixtures containing squalane in this study, all data points agree with the pure-solvent data within their uncertainties. Near infinite dilution, these agreements further suggest that the effect of CO_2 or propane on a is negligible, which is consistent with findings in the literature [25,32].

3.2.2. Influence of composition

Fig. 5 shows the thermal diffusivity a at $T = 293.15$ K as a function of x_{CO2} or $x_{propane}$ for the mixtures based on *n*-pentane (top), *n*-decane (middle), or squalane (bottom). For illustrating the influence of T on the composition dependence of a, results for the mixtures based on *n*-decane or squalane at $T = 333.15$ K are additionally shown. For comparison, Fig. 5 also includes a of the pure solvents, which were calculated as described in the previous section. For the mixture *n*-pentane/CO_2, a clearly tends to decrease with increasing x_{CO2}. This trend is consistent with the findings of Wu et al. [35], who observed a similar behavior for

Table 3
Thermal diffusivities a and Fick diffusion coefficients D_{11} as well as their relative experimental uncertainties ($k = 2$) determined by DLS for binary mixtures consisting of the solvents *n*-pentane, *n*-decane, *n*-hexadecane, or squalane and the solutes CO_2 or propane at different T[a], p[a] and Estimated x_{gas}[b].

T / K	p / MPa	x_{gas}	$10^9 \times a$ / (m^2s^{-1})	$100 \times U_r(a)$	$10^9 \times D_{11}$ / (m^2s^{-1})	$100 \times U_r(D_{11})$
n-pentane + CO_2						
293.10	0.375	0.057	78.1	5.6	9.7	11
293.07	0.973	0.15	76.4	4.5	9.71	4.1
293.06	1.859	0.28	72.1	3.4	8.42	7.3
293.06	3.053	0.46	65.6	4.5	7.47	5.5
313.48	0.476	0.054	72.5	2.5	12.84	6.1
313.42	1.166	0.13	70.0	3.3	11.60	4.7
332.99	0.830	0.075	68.1	4.8	15.8	9.4
333.01	1.375	0.12	66.2	4.5	14.32	4.3
352.82	1.008	0.076	61.1	2.3	17.0	12
352.81	1.621	0.12	61.4	8.1	17.1	12
372.91	1.478	0.10	56.4	4.9	19.9	9.0
373.30	1.908	0.13	55.7	8.5	20.0	11
392.80	1.778	0.12	55.5	6.9		
392.86	2.225	0.15	56	21		
n-pentane + propane						
293.08	0.105	0.054	77.4	2.2	7.06	11
293.06	0.141	0.095	78.0	1.6	7.20	10
293.04	0.287	0.26	78.2	2.5	7.29	8.5
293.07	0.514	0.51	76.8	2.5	7.92	6.1
313.48	0.186	0.056	71.7	2.6	8.4	12
332.94	0.302	0.052	68.0	2.8	10.38	7.2
352.85	0.502	0.057	62.9	2.0	14.1	11
373.63	0.739	0.044	58.1	3.5		
393.27	1.055	0.037	52.7	8.5		
n-decane + CO_2						
293.07	0.238	0.029	83.3	3.7	4.29	9.9
293.07	0.452	0.054	79.6	4.4	4.23	5.7
292.97	1.004	0.12	79.6	6.0	4.29	2.6
292.98	1.857	0.22	77.4	5.8	4.12	2.8
292.96	2.967	0.36	77.1	2.6	3.85	4.8
313.00	0.490	0.048	77.3	6.8	5.47	7.5
332.77	0.627	0.052	72.5	2.4	7.03	5.2
332.46	1.024	0.085	72.0	5.9	6.93	2.5
332.81	2.073	0.17	71.1	5.2	7.02	2.2
332.49	2.997	0.25	69.0	7.9	6.75	3.6
352.48	0.751	0.053	69.1	2.3	8.79	3.3
371.09	1.054	0.067	65.2	3.1	10.40	5.2
371.33	2.032	0.13	63.5	4.6	10.42	3.7
371.14	3.006	0.19	65.4	3.0	10.36	3.1
373.08	0.859	0.054	65.8	2.5	10.96	3.4
392.86	0.822	0.047	62.4	3.0	13.0	8.1
n-decane + propane						
293.09	0.043	0.055	80.7	3.1	2.50	7.9
293.05	0.083	0.11	80.2	4.1	2.50	8.7
293.03	0.124	0.16	80.7	4.2	2.66	4.1
293.07	0.155	0.20	81.1	3.6	2.78	4.5
293.12	0.265	0.34	79.3	9.7	3.03	5.9
313.04	0.065	0.055	75.4	2.5	3.44	7.0
332.82	0.092	0.048	73.1	3.3	4.28	9.3
333.06	0.410	0.22	71.2	3.1	4.76	3.8
333.05	0.212	0.11	71.4	3.5	4.65	4.2
333.07	0.572	0.30	72.2	5.4	5.03	4.6
352.33	0.121	0.04	69.9	2.2	5.91	7.2
372.01	0.217	0.050	64.4	6.0	6.77	11
373.32	0.441	0.10	62.4	6.9	7.15	4.4
373.28	0.822	0.19	64.2	5.9	7.61	6.5
373.52	1.008	0.24	63.5	4.0	7.71	5.5
391.55	0.254	0.050	63.1	5.1	8.73	10
n-hexadecane + propane						
293.06	0.052	0.051	87	13	1.112	7.9
313.45	0.073	0.052	83	15	1.71	6.8
332.97	0.092	0.049	75.5	4.9	2.29	12
352.60	0.119	0.048	74.1	6.4	3.08	11
373.18	0.151	0.047	69.8	8.7	4.13	8.4
392.71	0.184	0.049	66.2	9.9	5.23	11
squalane + CO_2						
293.05	0.222	0.052	77	21	0.755	5.9
293.07	0.677	0.16	78.1	10	0.8987	1.1
293.08	1.230	0.29	79	14	1.009	1.3
293.08	1.693	0.39	72.9	10	1.081	2.5
293.07	2.088	0.48	76.8	10	1.134	2.8
293.13	2.985	0.69	81.8	11	1.2230	3.5

(*continued on next page*)

Table 3 (*continued*)

T / K	p / MPa	x_{gas}	$10^9 \times a$ / (m^2s^{-1})	$100 \times U_r(a)$	$10^9 \times D_{11}$ / (m^2s^{-1})	$100 \times U_r(D_{11})$
313.16	0.248	0.047	73.7	11	1.377	6.9
333.14	0.334	0.053	72.0	9.3	2.23	12
332.71	1.068	0.17	74.2	11	2.314	3.8
332.73	2.255	0.36	71.4	9.3	2.445	2.8
332.52	3.195	0.51	71.0	13	2.478	2.2
352.48	0.344	0.048	69.8	11	3.16	4.6
373.34	0.366	0.047	67.7	9.2	4.18	7.3
373.41	1.243	0.16	63.7	6.9	4.26	5.8
372.93	2.163	0.28	66.1	9.3	4.30	2.8
373.44	3.124	0.40	64.0	8.6	4.389	1.2
392.76	0.377	0.046	64	17	5.16	8.4
squalane + propane						
293.04	0.039	0.068	73.8	10	0.254	14
293.09	0.100	0.18	77.5	8.1	0.308	5.4
293.05	0.247	0.44	80.6	12	0.496	4.9
313.41	0.054	0.070	75.4	13	0.479	16
332.94	0.068	0.064	71	27	0.870	6.5
332.92	0.142	0.13	70.6	9.7	0.951	5.7
332.92	0.227	0.21	70	17	1.038	4.3
333.20	0.461	0.43	68	26	1.2627	5.7
352.35	0.088	0.061	67.1	11	1.29	15
372.82	0.107	0.056	66.0	8.5	1.97	9.0
372.73	0.213	0.11	66.7	11	2.007	4.5
372.70	0.356	0.19	64.2	7.2	2.08	6.8
373.27	0.716	0.37	68	21	2.43	5.0
392.33	0.127	0.053	62.6	9.2	2.59	6.8

[a] Expanded uncertainty ($k = 2$) for T is 0.02 K and for p is 0.008 MPa.
[b] Amount fraction of the gas x_{gas} in the liquid phase is estimated using solubility data in the literature as detailed in Section 2.3.

mixtures of CO_2 dissolved in 1-hexanol. However, when CO_2 is substituted by propane in mixtures based on the solvent *n*-pentane, there is no such composition dependence and the values agree within combined uncertainties with a of the pure solvent. For mixtures based on *n*-decane or squalane with either CO_2 or propane as the solute, no clear composition dependence of a can be identified within the investigated range due to the larger experimental uncertainties. Additionally, the composition-dependent trend of a seems to be independent of T.

3.3. Fick diffusion coefficients

3.3.1. Influence of temperature at infinite dilution of the dissolved gas

Fig. 6 shows the Fick diffusion coefficients D_{11} for all binary mixtures investigated as part of this work at infinite dilution of the solutes, i.e. $x_{gas} \approx 0.05$. In the figure, different symbol types and colors represent mixtures with different solvents, while open and filled symbols indicate mixtures with the solutes CO_2 or propane. As a guideline for the eye, solid lines showing an Arrhenius-like correlation of D_{11} with respect to T for each mixture are given. For their determination, the data points were weighted by the inverse of their uncertainties in the correlation procedure. Fig. 6 further includes D_{11} data for mixtures consisting of *n*-hexadecane and CO_2 at infinite dilution from DLS measurements reported by Piszko et al. [25] for comparison. Considering all systems, D_{11} exhibits an Arrhenius-like increase with increasing T. For a given solute and at a specific T, the highest D_{11} value can be found for mixtures based

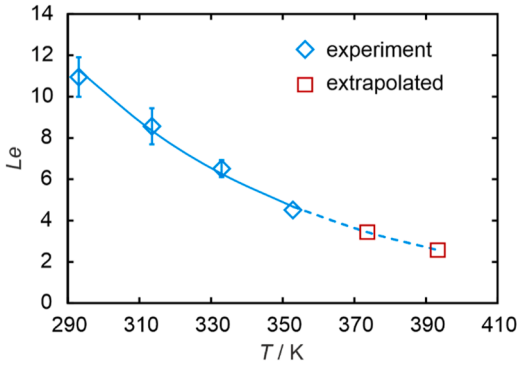

Fig. 3. Lewis numbers calculated by the thermal diffusivity and Fick diffusion coefficient data measured by DLS in this study for the binary mixture containing the solvent *n*-pentane and the solute propane as a function of T near infinite dilution. The state points where a reliable separation of the modes related to T and c fluctuations is possible are indicated by blue diamonds. The solid line represents an exponential fit for the resolved *Le*, while the dashed line shows its extrapolation to higher T. Red squares indicate the extrapolated values from the fit.

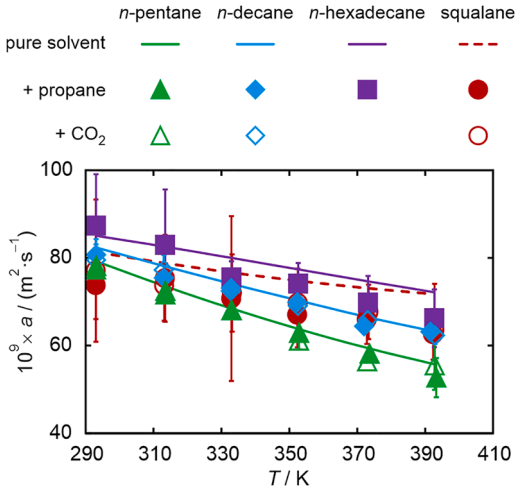

Fig. 4. Thermal diffusivity a from DLS measurements for binary mixtures consisting of *n*-pentane, *n*-decane, *n*-hexadecane, or squalane with dissolved CO_2 or propane as a function of T near infinite dilution ($x_{gas} \approx 0.05$). Open symbols represent mixtures with dissolved CO_2, while filled symbols denote those with dissolved propane. Different symbol types and colors indicate mixtures with varying solvents. Solid lines illustrate a of the pure solvents at p_{sat} obtained from equations of states for the solvents [13–15,27–29] taken from the REFPROP database [12]. The dashed line represents a of pure squalane, calculated using literature values for the thermal conductivity λ [30], density ρ [31], and heat capacity c_p [31] in the liquid phase.

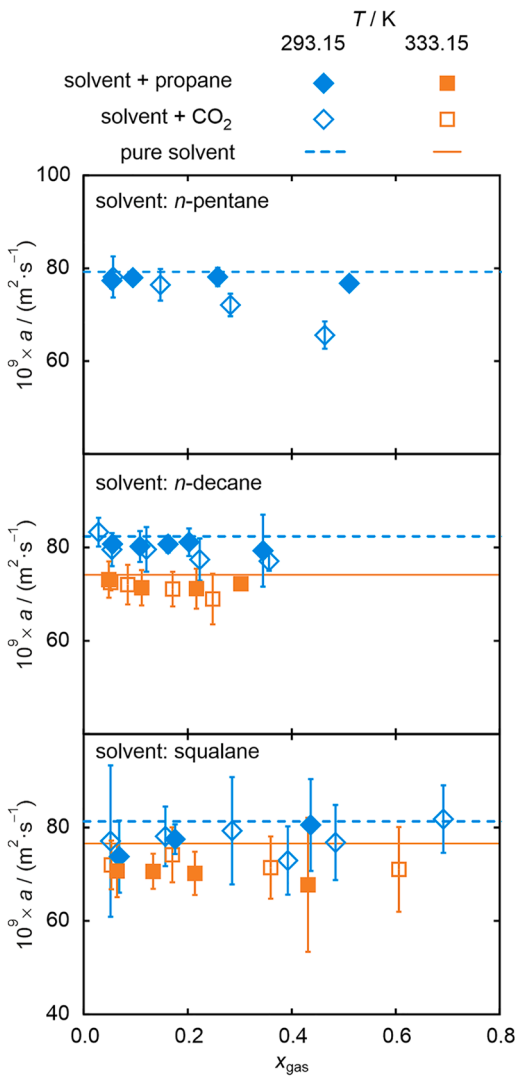

Fig. 5. Thermal diffusivity a from DLS experiments for binary mixtures based on *n*-pentane (top), *n*-decane (middle), or squalane (bottom) with dissolved CO_2 or propane as a function of x_{gas} at different T. Dashed lines indicate a of the pure solvents. Different symbol types and colors represent different T, while open and filled symbols refer to the solutes CO_2 or propane.

on the solvent *n*-pentane, followed by *n*-decane, and *n*-hexadecane, while the mixtures based on squalane show the lowest D_{11} values. This trend corresponds with the inverse correlation between solvent viscosity and D_{11} that is frequently addressed in the literature [3,36,37]. For a given solvent and at a given T, the mixtures containing CO_2 show larger D_{11} values than those containing propane. As the molar masses of both CO_2 and propane are very similar, the latter trend appears to be related to the difference in their molecular size. Here, propane possessing a larger molecular volume than CO_2 exhibits smaller D_{11} values. Such an inverse relationship between the solute volume and D_{11} has been reported in previous studies for systems with solvents in the form of *n*-alkanes [7], alcohols [3], and ionic liquids [33] and is also considered in available prediction models for D_{11} in the infinite dilution regime of the solute [38].

The results for D_{11} from this work can be compared to the results from Cadogan et al. [39], Guzmán and Garrido [40], and Grogan et al. [41]. Cadogan et al. [39] employed the Taylor dispersion method to measure D_{11} for binary mixtures of CO_2 dissolved in *n*-decane or squalane with typical relative uncertainties of 2.6%. Their experiments were conducted at T ranging from (298.15 to 423.15) K and p between (1 and

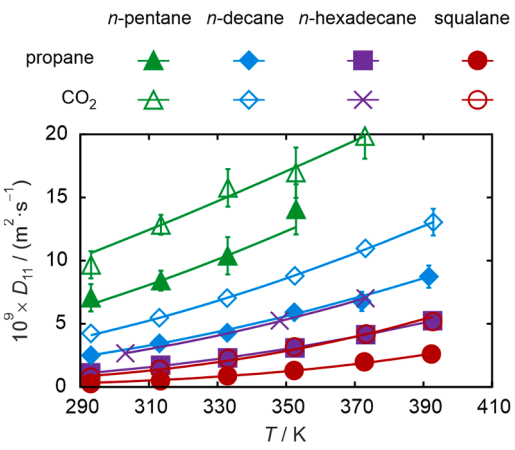

Fig. 6. Fick diffusion coefficient D_{11} from DLS measurements for binary mixtures consisting of the solvents *n*-pentane, *n*-decane, *n*-hexadecane, or squalane with dissolved CO_2 or propane as a function of T near infinite dilution ($x_{gas} \approx 0.05$). Solid lines show an Arrhenius-like correlation of the experimental data with respect to T as a guideline for the eye. Different symbol types and colors indicate mixtures with varying solvents. Open symbols represent mixtures with CO_2, while filled symbols denote those with propane. Cross symbols indicate data from Piszko et al. [25] for the mixture of CO_2 and *n*-hexadecane near infinite dilution.

69) MPa. To allow for a comparison, the D_{11} data from Cadogan et al. [39] as function of p at a given T were extrapolated to the saturation pressure, where D_{11} can be considered to be at infinite dilution of the dissolved gas. For the same purpose, the data from DLS at the lowest studied x_{gas} of approximately 0.05, as reported in Table 3, were correlated as a function of T using an Arrhenius-like fit, i.e. $D_{11} = A \cdot \exp^{-B/(R \cdot T)}$, where A and B are fitting parameters and R is the gas constant. The obtained D_{11} data from Cadogan et al. [39] agree with the results from this work with an AARD of 4.2%, which is within experimental uncertainties. Guzmán and Garrido [40] measured the self-diffusivity of CO_2 in *n*-decane using nuclear magnetic resonance (NMR) spectroscopy at gas pressures ranging from (0.1 to 0.65) MPa at $T = 298$ K with a relative uncertainty of 0.42%. Assuming that the conditions studied by them relate to infinite dilution of CO_2 in the liquid phase, the self-diffusivity of CO_2 can be considered to be equal to D_{11} [42], allowing for a valid comparison. Also here, the AARD of 5.5% of the literature values from the results measured within this work is within the experimental uncertainties of the DLS data. Grogan et al. [41] determined D_{11} of CO_2 in different hydrocarbons including *n*-pentane and *n*-decane from the volume swelling of the liquid phase during the solvation process. Since the reported data scatter considerably by up to 44%, a reliable extrapolation to the limit of infinite dilution of the dissolved gas was not possible.

3.3.2. *Influence of the composition*

Fig. 7 presents exemplarily D_{11} from this work as a function of the amount fraction of the dissolved gas x_{gas} for binary mixtures consisting of the solutes CO_2 or propane dissolved in the solvents *n*-pentane (top), *n*-decane (middle), or squalane (bottom) at $T \approx 293.15$ K. To highlight the impact of T on the relationship between D_{11} and x_{gas}, Fig. 7 also includes D_{11} data at $T \approx 333.15$ K. The open and closed symbols in Fig. 7 represent D_{11} of mixtures containing CO_2 and propane, while different symbol types and colors indicate different temperatures.

At $T \approx 293.15$ K, the system containing CO_2 and *n*-pentane shows constant D_{11} values as x_{CO2} increases up to 0.15. This behavior is likely associated with the limit of the infinite dilution range. Beyond this point, D_{11} begins to decrease with further increases in x_{CO2}. At the highest x_{CO2} investigated, D_{11} is approximately 23% smaller than the extrapolated value at infinite dilution. The observed behavior is counterintuitive, since the viscosity of the mixture is expected to decrease with increasing

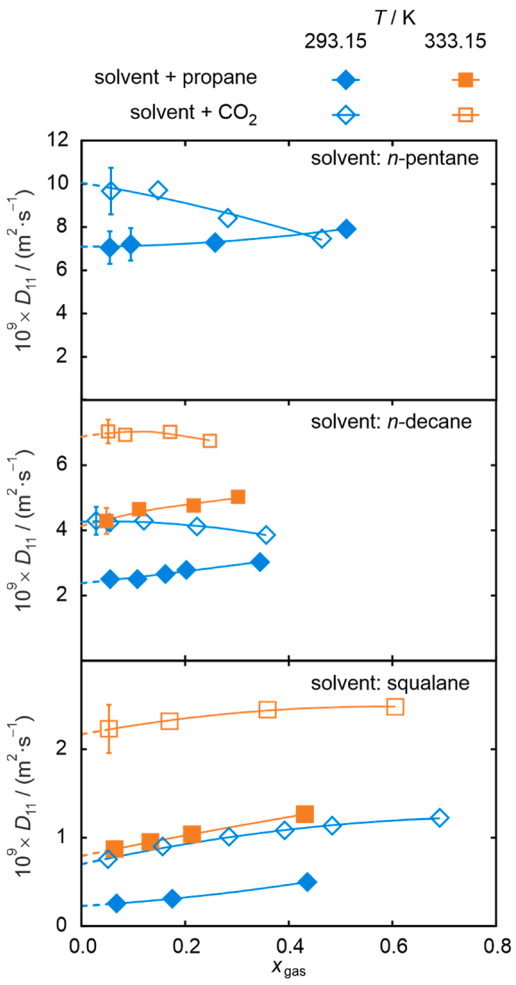

Fig. 7. Fick diffusion coefficient D_{11} from DLS experiments for binary mixtures containing the solvents *n*-pentane (top), *n*-decane (middle), or squalane (bottom) and the solutes CO_2 or propane as a function of x_{gas} at different *T*. Different symbol types and colors represent different *T* while open and filled symbols refer to the solutes CO_2 and propane. Solid lines represent fits of polynomial functions up to second order to the experimental data. Dashed lines show the extrapolation of the fit to infinite dilution.

x_{CO2} according to calculations within the REFPROP database [12]. Usually, a decrease in viscosity suggests decreasing strength of molecular interactions, which in turn may be expected to lead to an increase in D_{11}. Therefore, the decrease of D_{11} with increasing x_{CO2} is likely due to distinct structural changes in the liquid phase. Previous studies have documented a similar decrease of D_{11} in mixtures of CO_2 dissolved in various alkanes with low carbon numbers, such as *n*-hexane [43] or cyclohexane [25]. Using Raman spectroscopy and molecular dynamics (MD) simulations, these studies have linked this behavior to the formation of CO_2 clusters in the liquid phase, which hinders the Fickian diffusion process.

Considering the mixtures containing *n*-decane and CO_2 at $T \approx 293.15$ K, D_{11} shows nearly constant values over the investigated composition range, with a slightly decreasing tendency with increasing x_{CO2} above $x_{CO2} = 0.12$ within the experimental uncertainties. At elevated *T*, D_{11} is independent of the composition within the investigated x_{CO2} range. These behaviors are likely due to a complex interplay between fluid structures and system dynamics as observed for mixtures containing CO_2 and alkanes like *n*-hexadecane by Piszko et al. [25]. In comparison to short-chain alkanes like *n*-pentane, a greater reduction in mixture viscosity by the solvation of CO_2 can be expected in *n*-decane due to the larger difference in the pure-component viscosities. This is supported by

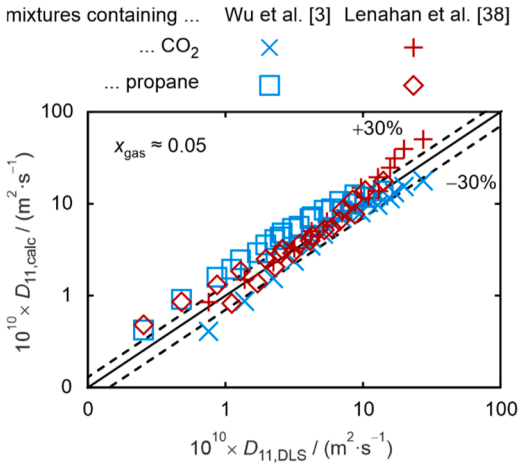

Fig. 8. Comparison of $D_{11,calc}$ data calculated using the prediction models given by Wu et al. [3] (blue color) and Lenahan et al. [38] (red color) and $D_{11,DLS}$ data from the present DLS measurements near infinite dilution of the dissolved gas. The solid line indicates a perfect agreement while dashed lines denote deviations of ±30% of $D_{11,calc}$ from $D_{11,DLS}$.

the viscosity data of Kian and Scurto [44] for the mixtures of *n*-decane or *n*-hexane with dissolved CO_2. Even though CO_2 clusters may form in *n*-decane, which potentially hinders the diffusion process, the considerable reduction in η of the mixture can facilitate mass transfer. These opposing effects seem to compensate for each other and lead to nearly invariant D_{11} values across the investigated range of x_{CO2} in mixtures based on *n*-decane.

In contrast to the two mixtures discussed before, D_{11} of the binary mixture of squalane with dissolved CO_2 increases with increasing x_{CO2}. At $T \approx 293.15$ K, D_{11} at $x_{CO2} \approx 0.70$ is approximately 62% larger than that at infinite dilution. Also this trend may be explained with the interplay of the two opposing effects of the mixture viscosity and the formation of CO_2 clusters. Since squalane has the largest pure-component viscosity of all investigated solvents, it seems reasonable that the influence of decreasing mixture viscosity with increasing x_{CO2} dominates over the effect of CO_2 clustering and, consequently, leads to an increase of D_{11}. This agrees with previous experimental investigations by Piszko et al. [25] who have reported similar increasing trends for D_{11} in binary mixtures of CO_2 dissolved in long linear alkanes, such as *n*-octacosane. Based on the analysis of Raman spectra and the calculation of the thermodynamic factors, they have attributed the increase of D_{11} with increasing x_{CO2} to the breakdown of the solvent network, facilitating the diffusion process. The observations also agree with the results of Zabala et al. [45], who calculated the thermodynamic factors via the PC-SAFT equation of state in connection with their study of diffusion in mixtures of CO_2 dissolved in various alkanes ranging from *n*-dodecane to *n*-tetracontane. With increasing x_{CO2}, the authors found increasing thermodynamic factors from values below unity for the mixtures with *n*-dodecane to values above unity for those with long linear alkanes like *n*-octacosane or *n*-tetracontane, which also indicates an increasing D_{11} with increasing x_{CO2} as it was observed for the mixture of squalane and CO_2 in this work. A comparison of the composition-dependent trend for D_{11} of this mixture at the two investigated *T* indicates a negligible influence of *T*.

The filled symbols in Fig. 7 indicate that for all mixtures containing the solute propane, D_{11} tends to increase with increasing $x_{propane}$ at a given *T*. Thus, it seems that the inverse relation between the composition-dependent mixture viscosity and D_{11} observed in previous studies on similar systems [6] also applies here. In comparison to CO_2, a clustering of propane in the solvents studied is much less likely due to their similar molecular characteristics. Among the corresponding mixtures studied, the influence of $x_{propane}$ on D_{11} tends to increase from the

systems containing *n*-pentane over *n*-decane to squalane. This is reasonable since the difference between the viscosities of the pure solvent and propane increases in the same order. Also for mixtures containing propane as the solute, the influence of T on the composition-dependent trend of D_{11} is negligible.

3.3.3. Prediction of the Fick diffusion coefficient at infinite dilution

To test whether the D_{11} data at infinite dilution of the dissolved gas for the binary mixtures studied in this work correspond with respective prediction methods, two such models were tested. Both models were developed at the Institute of Advanced Optical Technologies – Thermophysical Properties (AOT-TP) specifically for predicting D_{11} in mixtures consisting of liquids with dissolved gases and have shown a good prediction performance for a large variety of different solute-solvent combinations [3,38].

The semi-empirical model proposed by Wu et al. [3] was originally developed to estimate D_{11} in binary mixtures of primary alcohols and linear alkanes with the dissolved gases hydrogen (H_2), helium (He), nitrogen (N_2), carbon monoxide (CO), and CO_2 at infinite dilution. As input properties, only T, the molar masses of the solvent and the solute, the kinematic viscosity and dipole moment of the pure solvent, and the acentric factor of the solute are required. Here, the acentric factor was incorporated to account for the sphericity of the solute and the fact that H_2, even though it is lighter than He, often diffuses more slowly due to its larger size. For the application of this model for the systems studied here, the dipole moments for *n*-pentane and *n*-decane were set to 0.07 Debye and those for *n*-hexadecane and squalane were set to 0 Debye following the recommendation of Harvey and Lemmon [46]. Data for the kinematic viscosity of *n*-pentane, *n*-decane, and *n*-hexadecane were obtained from the REFPROP database [12] based on Refs. [47–59]. For squalane, the kinematic viscosity was calculated via density and dynamic viscosity data from Mylona et al. [60]. The acentric factors of the solutes were taken from the REFPROP database [12].

The second model considered here was introduced by Lenahan et al. [38], after a comprehensive review of existing models for predicting D_{11} in binary mixtures of liquids with dissolved gases at infinite dilution with a special focus on asymmetric mixtures. This transferable model is based on a dataset of 451 experimental measurements across a wide range of solvents, including hydrocarbons, alcohols, acids, ethers, and ionic liquids, and of solutes, including He, H_2, N_2, CO, CO_2, and some refrigerants. As input parameters, the model requires T, the density, dynamic viscosity, and molecular mass of the solvent, and the molar core volumes of the solvent and solute. The molar core volume reflects the effective three-dimensional space occupied by a molecule, determined based on its structure and interactions. For the present mixtures, the molar core volumes for *n*-decane, *n*-hexadecane, and CO_2 were taken from Lenahan et al. [38], while values for propane, *n*-pentane, and squalane were calculated on the basis of overlapping spheres representing the atom core volumes, as detailed in the aforementioned publication.

Fig. 8 presents a parity plot comparing the predicted $D_{11,calc}$ values from the models proposed by Wu et al. [3] and Lenahan et al. [38] with the experimental D_{11} data from this work at $x_{gas} \approx 0.05$.

The model by Wu et al. [3] achieves an overall AARD from the experimental data of 41%, with clearly different performances for the different solutes. While the AARD is only 18% for the CO_2-based systems, it is 61% for the propane-based mixtures. Individual deviations range from 0.26% for *n*-decane/CO_2 at $T = 293$ K to as high as 91% for squalane/propane at $T = 352$ K. The better agreement for CO_2-based mixtures can be explained by the fact that mixtures consisting of alkanes with dissolved CO_2 were part of the training set. Notably, all D_{11} values for the CO_2-based mixtures are underpredicted. In contrast, the model shows a consistent overprediction for propane-based mixtures. The larger deviations for the propane-based mixtures might be related to the fact that only smaller solutes were part of the training set and that the model does not consider the volume of the solute molecules explicitly.

In contrast, the model given by Lenahan et al. [38] shows better overall performance, where the total AARD is 27%. It achieves AARDs of 30% for CO_2-based mixtures and 25% for propane-based mixtures. The deviations range from 0.65% for *n*-hexadecane/propane at $T = 392$ K to 99% for *n*-pentane/CO_2 at $T = 373$ K. The large deviations observed within group of CO_2-based systems are primarily due to the mixture consisting of CO_2 and *n*-pentane, where the model predicts D_{11} with an AARD of 71%. For *n*-decane/CO_2 and squalane/CO_2, the AARD is 9.5% and, thus, significantly lower.

In summary, the comparison shows that the model proposed by Wu et al. [3] performs well in predicting diffusion coefficients in CO_2-based mixtures, but shows considerable deviations for the propane-based systems. Although the model given by Lenahan et al. [38] exhibits larger deviations for specific cases like for the *n*-pentane/CO_2 system, it provides more consistent and accurate predictions across the studied systems.

4. Conclusions

The present work reports thermal diffusivity a and Fick diffusion coefficient D_{11} data measured by DLS experiments in the saturated liquid phases of binary mixtures consisting of the solvents *n*-pentane, *n*-decane, *n*-hexadecane, or squalane with dissolved propane or CO_2 at T between (293 and 393) K and x_{gas} between 0.029 and 0.69 with average expanded experimental uncertainties ($k = 2$) of 7.6% and 6.6%. For a, the results for the binary mixtures agreed in most cases within combined uncertainties with literature data for the pure solvents. Only for the mixture consisting of *n*-pentane and CO_2, a significant decrease of a with increasing amount of dissolved CO_2 with a maximum reduction of 15% at $x_{CO2} = 0.46$ was observed. For D_{11}, good agreement with the scarce amount of experimental data available in the literature was found. At a given T at infinite dilution of the dissolved gas, D_{11} in CO_2-based mixtures is larger than in propane-based mixtures in the same solvent, which may be explained by the larger size of propane that hinders the movement of propane molecules within the fluid structure. For mixtures with the same solute at infinite dilution in different solvents at a given T, the inverse relationship between D_{11} and the solvent viscosity that is often reported in the literature was confirmed [3,36,37]. The composition-dependent trend of D_{11} varies for the different systems studied, which can be explained by the superposition of two opposing effects. These are decreasing mixture viscosities with increasing x_{gas}, associated with an increase in D_{11}, and the increasing formation of solute clusters with increasing x_{gas}, which is much more relevant for the solute CO_2 and leads to a decrease in D_{11}. The experimental D_{11} data at infinite dilution of the gas from this work were further used to evaluate the performance of two corresponding prediction models. Here, the model proposed by Lenahan et al. [38] performs best and yields an AARD of 27% from all infinite-dilution D_{11} data from the present study.

Funding

This work was funded by the Deutsche Forschungsgemeinschaft (DFG, German Research Foundation) via Project Grant FR1709/28–1 within the Research Unit FOR 5595 Archimedes (Oil-refrigerant multiphase flows in gaps with moving boundaries—Novel microscopic and macroscopic approaches for experiment, modeling, and simulation)—Project Number 510921053.

CRediT authorship contribution statement

Chathura J. Kankanamge: Writing – review & editing, Writing – original draft, Investigation, Data curation. **Paul Damp:** Writing – review & editing, Writing – original draft, Investigation. **Thomas M. Koller:** Writing – review & editing. **Michael H. Rausch:** Writing – review & editing. **Dominik Krug:** Writing – review & editing. **Wolfgang Schröder:** Writing – review & editing. **Tobias Klein:** Writing – review &

editing, Writing – original draft, Supervision, Conceptualization. **Andreas P. Fröba:** Writing – review & editing, Supervision, Funding acquisition, Conceptualization.

Declaration of competing interest

The authors declare that they have no known competing financial interests or personal relationships that could have appeared to influence the work reported in this paper.

Acknowledgements

The authors gratefully acknowledge funding of the Erlangen Graduate School in Advanced Optical Technologies (SAOT) by the Bavarian State Ministry for Science and Art.

Supplementary materials

Supplementary material associated with this article can be found in the online version at doi:10.1016/j.fluid.2025.114429.

Data availability

The primary data is provided as supplementary information.

References

[1] R. Pecora, Dynamic Light Scattering: Applications of Photon Correlation Spectroscopy, Springer, New York, USA, 1985.
[2] M. Piszko, C. Giraudet, A.P. Fröba, Diffusivities of an equimolar methane–propane mixture across the two-phase region by dynamic light scattering, Int. J. Thermophys. 41 (2020) 102, https://doi.org/10.1007/s10765-020-02680-1.
[3] W. Wu, T. Klein, M. Kerscher, M.H. Rausch, T.M. Koller, C. Giraudet, A.P. Fröba, Diffusivities in 1-alcohols containing dissolved H_2, He, N_2, CO, or CO_2 close to infinite dilution, J. Phys. Chem. B 123 (2019) 8777–8790, https://doi.org/10.1021/acs.jpcb.9b06211.
[4] R.N. O'Brien, D. Quon, Refractive index of some alcohols and saturated hydrocarbons at 6328 A, J. Chem. Eng. Data 13 (1968) 517, https://doi.org/10.1021/je60039a017.
[5] M.L.L. Paredes, R.A. Reis, A.A. Silva, R.N.G. Santos, G.J. Santos, Densities, sound velocities, and refractive indexes of tetralin + *n*-hexadecane at (293.15, 303.15, 313.15, 323.15, 333.15, and 343.15) K, J. Chem. Eng. Data 56 (2011) 4076–4082, https://doi.org/10.1021/je200504u.
[6] N. Tripathi, Densities, viscosities, and refractive indices of mixtures of hexane with cyclohexane, decane, hexadecane, and squalane at 298.15 K, Int. J. Thermophys. 26 (2005) 693–703, https://doi.org/10.1007/s10765-005-5572-8.
[7] C. Giraudet, T. Klein, G. Zhao, M.H. Rausch, T.M. Koller, A.P. Fröba, Thermal, mutual, and self-diffusivities of binary liquid mixtures consisting of gases dissolved in *n*-alkanes at infinite dilution, J. Phys. Chem. B 122 (2018) 3163–3175, https://doi.org/10.1021/acs.jpcb.8b00733.
[8] A.P. Fröba, Dynamic light scattering (DLS) for the characterization of working fluids in chemical and energy engineering, Habilitation Thesis, Friedrich-Alexander-Universität Erlangen-Nürnberg (FAU), Erlangen, Germany, 2009.
[9] T.M. Koller, M.H. Rausch, A.P. Fröba, Dynamic light scattering for the measurement of transport properties of fluids, Int. J. Thermophys. 45 (2024) 57, https://doi.org/10.1007/s10765-024-03344-0.
[10] M. Piszko, T. Schaible, C. Bonten, A.P. Fröba, Mutual and thermal diffusivities in polystyrene melts with dissolved nitrogen by dynamic light scattering, Macromolecules 54 (2021) 5662–5672, https://doi.org/10.1021/acs.macromol.1c00819.
[11] J.M.O. De Zarate, J.V Sengers, Hydrodynamic Fluctuations in Fluids and Fluid Mixtures, Elsevier, Amsterdam, Netherlands, 2006.
[12] E.W. Lemmon, I.H. Bell, M.L. Huber, M.O. McLinden, NIST Standard Reference Database 23: Reference Fluid Thermodynamic and Transport Properties-REFPROP, Version 10.0, National Institute of Standards and Technology, Standard Reference Data Program, Gaithersburg, USA, 2018.
[13] M. Thol, T. Uhde, E.W. Lemmon, R. Span, Fundamental equations of state for hydrocarbons. Part I. *n*-Pentane, to be published.
[14] E.W. Lemmon, R. Span, Short fundamental equations of state for 20 industrial fluids, J. Chem. Eng. Data 51 (2006) 785–850, https://doi.org/10.1021/je050186n.
[15] R. Romeo, E.W. Lemmon, Helmholtz equation of state for hexadecane, to be published (2018).
[16] A. Zafar, J. Chickos, The vapor pressure and vaporization enthalpy of squalene and squalane by correlation gas chromatography, J. Chem. Thermodyn. 135 (2019) 192–197, https://doi.org/10.1016/j.jct.2019.03.032.
[17] C. Tsonopoulos, Thermodynamic analysis of the mutual solubilities of normal alkanes and water, Fluid Phase Equilib. 156 (1999) 21–33, https://doi.org/10.1016/S0378-3812(99)00021-7.
[18] H. Cheng, M.E. Pozo de Fernandez, J.A. Zollweg, W.B. Streett, Vapor-liquid equilibrium in the system carbon dioxide + *n*-pentane from 252 to 458 K at pressures to 10 MPa, J. Chem. Eng. Data 34 (1989) 319–323, https://doi.org/10.1021/je00057a018.
[19] H.H. Reamer, B.H. Sage, Phase equilibria in hydrocarbon systems. Volumetric and phase behavior of the *n*-decane-CO_2 system, J. Chem. Eng. Data 8 (1963) 508–513, https://doi.org/10.1021/je60019a010.
[20] C.P. Chai, M.E. Paulaitis, Gas solubilities of carbon dioxide in heavy hydrocarbons, J. Chem. Eng. Data 26 (1981) 277–279, https://doi.org/10.1021/je00025a016.
[21] J. Vejrosta, I. Wichterle, The propane-pentane system at high pressures, Collect. Czechoslov. Chem. Commun. 39 (1974) 1246–1248, https://doi.org/10.1135/cccc19741246.
[22] H.H. Reamer, B.H. Sage, Phase equilibria in hydrocarbon systems. Volumetric and phase behavior of the propane-*n*-decane system, J. Chem. Eng. Data 11 (1966) 17–24, https://doi.org/10.1021/je60028a004.
[23] M. Zuliani, A. Barreau, J. Vidal, P. Alessi, M. Fenneglia, Measurements, correlation and prediction of Henry's constants of light alkanes in model heavy hydrocarbons and petroleum fractions, Fluid Phase Equilib. 82 (1993) 141–148, https://doi.org/10.1016/0378-3812(93)87137-P.
[24] H. Hong, M. Gong, J. Wu, Solubility measurements of 1,1,1,2-tetrafluoroethane (R134a) and of propane in squalane at temperatures from (325 to 400) K and pressures from (0.1 to 1) MPa, J. Chem. Eng. Data 51 (2006) 2270–2273, https://doi.org/10.1021/je060330k.
[25] M. Piszko, F.D. Lenahan, L. Friedl, T. Klein, A.P. Fröba, Mutual and thermal diffusivities in mixtures of cyclohexane, *n*-hexadecane, *n*-octacosane, or *n*-hexanoic acid with carbon dioxide obtained by dynamic light scattering and molecular dynamics simulations, J. Chem. Eng. Data 67 (2022) 3059–3076, https://doi.org/10.1021/acs.jced.2c00487.
[26] M. Piszko, K. Batz, M.H. Rausch, C. Giraudet, A.P. Fröba, Diffusivities of binary mixtures consisting of carbon dioxide, methane, and propane by dynamic light scattering, J. Chem. Eng. Data 65 (2020) 1068–1082, https://doi.org/10.1021/acs.jced.9b00495.
[27] C.M. Vassiliou, M.J. Assael, M.L. Huber, R.A. Perkins, Reference correlations of the thermal conductivity of cyclopentane, iso-pentane, and *n*-pentane, J. Phys. Chem. Ref. Data 44 (2015) 33102, https://doi.org/10.1063/1.4927095.
[28] M.L. Huber, R.A. Perkins, Thermal conductivity correlations for minor constituent fluids in natural gas: *n*-octane, *n*-nonane and *n*-decane, Fluid Phase Equilib. 227 (2005) 47–55, https://doi.org/10.1016/j.fluid.2004.10.031.
[29] S.A. Monogenidou, M.J. Assael, M.L. Huber, Reference correlation for the thermal conductivity of *n*-hexadecane from the triple point to 700 K and up to 50 MPa, J. Phys. Chem. Ref. Data 47 (2018) 13103, https://doi.org/10.1063/1.5021459.
[30] F.E. Berger Bioucas, M.H. Rausch, T.M. Koller, A.P. Fröba, Thermal conductivity of liquid cyclohexane, *n*-decane, *n*-hexadecane, and squalane at atmospheric pressure up to 353 K determined with a steady-state parallel-plate instrument, Int. J. Thermophys. 45 (2024) 93, https://doi.org/10.1007/s10765-024-03383-7.
[31] V.I. Korotkovskii, A.V Lebedev, O.S. Ryshkova, M.F. Bolotnikov, Y.E. Shevchenko, Y.A. Neruchev, Thermophysical properties of liquid squalane $C_{30}H_{62}$ within the temperature range of 298.15–413.15 K at atmospheric pressure, High Temp. 50 (2012) 471–474, https://doi.org/10.1134/S0018151X12040116.
[32] F.D. Lenahan, M. Piszko, T. Klein, A.P. Fröba, Diffusivities in binary mixtures of *n*-decane, *n*-hexadecane, *n*-octacosane, 2-methylpentane, 2,2-dimethylbutane, cyclohexane, benzene, ethanol, 1-decanol, ethyl butanoate, or *n*-hexanoic acid with dissolved He or Kr close to infinite dilution, J. Chem. Eng. Data 67 (2022) 622–635, https://doi.org/10.1021/acs.jced.1c00922.
[33] T. Klein, M. Piszko, M. Lang, J. Mehler, P.S. Schulz, M.H. Rausch, C. Giraudet, T. M. Koller, A.P. Fröba, Diffusivities in binary mixtures of [AMIM][NTf_2] ionic liquids with the dissolved gases H_2, He, N_2, CO, CO_2, or Kr close to infinite dilution, J. Chem. Eng. Data 65 (2020) 4116–4129, https://doi.org/10.1021/acs.jced.0c00430.
[34] M. Piszko, F.D. Lenahan, S. Hahn, M.H. Rausch, T.M. Koller, T. Klein, A.P. Fröba, Diffusivities in binary mixtures of *n*-hexane or 1-hexanol with dissolved CH_4, Ne, Kr, R143a, SF_6, or R236fa close to infinite dilution, J. Chem. Eng. Data 66 (2021) 2218–2232, https://doi.org/10.1021/acs.jced.1c00084.
[35] W. Wu, T. Klein, M. Kerscher, M.H. Rausch, T.M. Koller, C. Giraudet, A.P. Fröba, Mutual and thermal diffusivities as well as fluid-phase equilibria of mixtures of 1-hexanol and carbon dioxide, J. Phys. Chem. B 124 (2020) 2482–2494, https://doi.org/10.1021/acs.jpcb.0c00646.
[36] E.L. Cussler, Multicomponent Diffusion, Elsevier Scientific Publishing Company, Amsterdam, Netherlands, 1976.
[37] C.R. Wilke, P. Chang, Correlation of diffusion coefficients in dilute solutions, AlChE J 1 (1955) 264–270, https://doi.org/10.1002/aic.690010222.
[38] F.D. Lenahan, M. Piszko, T. Klein, A.P. Fröba, Prediction of Fick diffusion coefficients in binary mixtures of liquids with dissolved gases at infinite dilution-A review, J. Chem. Eng. Data 69 (2024) 692–702, https://doi.org/10.1021/acs.jced.3c00618.
[39] S.P. Cadogan, B. Mistry, Y. Wong, G.C. Maitland, J.P.M. Trusler, Diffusion coefficients of carbon dioxide in eight hydrocarbon liquids at temperatures between (298.15 and 423.15) K at pressures up to 69 MPa, J. Chem. Eng. Data 61 (2016) 3922–3932, https://doi.org/10.1021/acs.jced.6b00691.
[40] J. Guzmán, L. Garrido, Determination of carbon dioxide transport coefficients in liquids and polymers by NMR spectroscopy, J. Phys. Chem. B 116 (2012) 6050–6058, https://doi.org/10.1021/jp302037w.

[41] A.T. Grogan, V.W. Pinczewski, G.J. Ruskauff, F.M. Orr, Diffusion of CO_2 at reservoir conditions: models and measurements, SPE Reserv. Eng. 3 (1988) 93–102, https://doi.org/10.2118/14897-PA.
[42] X. Liu, S.K. Schnell, J.M. Simon, P. Krüger, D. Bedeaux, S. Kjelstrup, A. Bardow, T. J.H. Vlugt, Diffusion coefficients from molecular dynamics simulations in binary and ternary mixtures, Int. J. Thermophys. 34 (2013) 1169–1196, https://doi.org/10.1007/s10765-013-1482-3.
[43] T. Klein, W. Wu, M.H. Rausch, C. Giraudet, T.M. Koller, A.P. Fröba, Influence of liquid structure on Fickian diffusion in binary mixtures of *n*-hexane and carbon dioxide probed by dynamic light scattering, Raman spectroscopy, and molecular dynamics simulations, J. Phys. Chem. B 122 (2018) 7122–7133, https://doi.org/10.1021/acs.jpcb.8b03568.
[44] K. Kian, A.M. Scurto, Viscosity of compressed CO_2-saturated *n*-alkanes: CO_2/*n*-hexane, CO_2/*n*-decane, and CO_2/*n*-tetradecane, J. Supercrit. Fluids 133 (2018) 411–420, https://doi.org/10.1016/j.supflu.2017.10.030.
[45] D. Zabala, C. Nieto-Draghi, J.C. de Hemptinne, A.L. López de Ramos, Diffusion coefficients in CO_2/*n*-alkane binary liquid mixtures by molecular simulation, J. Phys. Chem. B 112 (2008) 16610–16618, https://doi.org/10.1021/jp8042329.
[46] A.H. Harvey, E.W. Lemmon, Method for estimating the dielectric constant of natural gas mixtures, Int. J. Thermophys. 26 (2005) 31–46, https://doi.org/10.1007/s10765-005-2351-5.
[47] M.L. Huber, Models For viscosity, thermal conductivity, and surface tension of selected pure fluids as implemented in REFPROP v10.0, National Institute of Standards and Technology, Boulder, CO, 2018, https://doi.org/10.6028/NIST.IR.8209.
[48] C.M.B.P. Oliveira, W.A. Wakeham, The viscosity of five liquid hydrocarbons at pressures up to 250 MPa, Int. J. Thermophys. 13 (1992) 773–790, https://doi.org/10.1007/BF00503906.
[49] D.R. Caudwell, J.P.M. Trusler, V. Vesovic, W.A. Wakeham, The viscosity and density of *n*-dodecane and *n*-octadecane at pressures up to 200 MPa and temperatures up to 473 K, Int. J. Thermophys. 25 (2004) 1339–1352. https://doi.org/10.1007/s10765-004-5742-0.
[50] S. Sotiriadou, E. Ntonti, M.J. Assael, M.L. Huber, Reference correlations of the viscosity and thermal conductivity of 1-hexene from the triple point to high temperatures and pressures, Int. J. Thermophys. 44 (2023) 108, https://doi.org/10.1007/s10765-023-03217-y.
[51] A. Estrada-Baltazar, G.A. Iglesias-Silva, M.A. Barrufet, Liquid viscosities of pentane and pentane + decane from 298.15 K to 373.15 K and up to 25 MPa, J. Chem. Eng. Data 43 (1998) 601–604, https://doi.org/10.1021/je9702697.
[52] F. Audonnet, A.A.H. Pádua, Simultaneous measurement of density and viscosity of *n*-pentane from 298 to 383 K and up to 100 MPa using a vibrating-wire instrument, Fluid Phase Equilib. 181 (2001) 147–161, https://doi.org/10.1016/S0378-3812(01)00487-3.
[53] B. Tohidi, R.W. Burgass, A. Danesh, A.C. Todd, Viscosity and density of methane + methylcyclohexane from (323 to 423) K and pressures to 140 MPa, J. Chem. Eng. Data 46 (2001) 385–390, https://doi.org/10.1021/je000191l.
[54] P. Ma, Q. Zhou, C. Yang, S. Xia, Measurement of viscosities and densities of liquids by vibrating-wire method, J. Chem. Ind. Eng. 55 (2004) 1608–1613. China.
[55] M.L. Huber, A. Laesecke, H.W. Xiang, Viscosity correlations for Minor constituent fluids in natural gas: *n*-octane, *n*-nonane and *n*-decane, Fluid. Phase Equilib. 228–229 (2005) 401–408, https://doi.org/10.1016/j.fluid.2005.03.008.
[56] B. Knapstad, P.A. Skjoelsvik, H.A. Oeye, Viscosity of pure hydrocarbons, J. Chem. Eng. Data 34 (1989) 37–43, https://doi.org/10.1021/je00055a013.
[57] B. Knapstad, P.A. Skjoelsvik, H.A. Oeye, Viscosity of three binary hydrocarbon mixtures, J. Chem. Eng. Data 36 (1991) 84–88, https://doi.org/10.1021/je00001a025.
[58] J.H. Dymond, K.J. Young, Transport properties of nonelectrolyte liquid mixtures—I. Viscosity coefficients for *n*-alkane mixtures at saturation pressure from 283 to 378 K, Int. J. Thermophys. 1 (1980) 331–344, https://doi.org/10.1007/BF00516562.
[59] X.Y. Meng, Y.K. Sun, F.L. Cao, J.T. Wu, V. Vesovic, Reference correlation of the viscosity of n-hexadecane from the triple point to 673 K and up to 425 MPa, J. Phys. Chem. Ref. Data 47 (2018) 033102, https://doi.org/10.1063/1.5039595.
[60] S.K. Mylona, M.J. Assael, K.D. Antoniadis, S.K. Polymatidou, L. Karagiannidis, Measurements of the viscosity of bis(2-ethylhexyl) sebacate, squalane, and bis(2-ethylhexyl) phthalate between (283 and 363) K at 0.1 MPa, J. Chem. Eng. Data 58 (2013) 2805–2808, https://doi.org/10.1021/je4005245.